Journal of Magnetism and Magnetic Materials 324 (2012) 534–539

Contents lists available at SciVerse ScienceDirect

Journal of Magnetism and Magnetic Materials

journal homepage: www.elsevier.com/locate/jmmm

Synthesis and functionalization of magnetite nanoparticles with different amino-functional alkoxysilanes

Rafael A. Bini [a,*], Rodrigo Fernando C. Marques [b], Francisco J. Santos [a], Juliano A. Chaker [c], Miguel Jafelicci Jr.[a]

[a] Institute of Chemistry, Laboratory of Magnetic Materials and Colloids, São Paulo State University—UNESP, Caixa Postal 355, Araraquara 14800-900, Brazil
[b] Institute of Science and Technology, Alfenas Federal University, Poços de Caldas 37701-100, Brazil
[c] FCE, Brasília University, Caixa Postal 7380, Brasília 72220-140, Brazil

ARTICLE INFO

Article history:
Received 10 February 2011
Received in revised form
25 July 2011
Available online 26 August 2011

Keywords:
Magnetite
Superparamagnetism
Magnetic measurement
Surface functionalization
Electrokinetic measurement

ABSTRACT

Superparamagnetic iron oxide (SPIO) nanoparticles show great promise for many biotechnological applications. This paper addresses the synthesis and characterization of SPIO nanoparticles grafted with three different alkoxysilanes: 3-aminopropyl-triethoxysilane (APTES), 3-aminopropyl-ethyl-diethoxy-silane (APDES) and 3-aminopropyl-diethy-ethoxysilane (APES). SPIO nanoparticles with an average particle diameter of 10 nm were prepared by chemical sonoprecipitation. As confirmed by Fourier transform infrared (FTIR) spectroscopy, silylation of these nanoparticles occurs through a two-step process. Decreasing the number of alkoxide groups reduced the concentration of free amino groups on the SPIO surface ([SPIO-NH_2]—APTES > APDES > APES). This phenomenon results from steric contributions and the formation of H-bonded amines provided by the ethyl groups present in the APDES and APES molecules. A simulation of SPIO nanoparticles in a saline physiologic solution shows that the ethyl groups impart larger steric stability onto the ferrofluids, which reduces aggregation. The magnetization (M) versus magnetic field (H) curves show that the synthesized iron oxide nanoparticles display superparamagnetic behavior. The zero-field cooling (ZFC) and field cooling (FC) curves show that the changes in the blocking temperature depend on the alkoxysilane-functionalized particle surface.

1. Introduction

Nanoscale magnetic materials have generated significant interest in recent years. Investigations of iron oxides (Fe_3O_4 and γ-Fe_2O_3), synthesized by several methods and functionalized for different applications, are being increasingly reported in the literature. This increased interest is partly due to the simplicity of preparing nanoparticles and their stable storage in the colloidal form. Colloidal suspensions of stabilized magnetic nanoparticles are called ferrofluids. These ferrofluids can interact with a magnetic field [1]. The development and the understanding of superparamagnetic iron oxide (SPIO) nanoparticles dispersions are becoming more important for biomedical applications. SPIO is constituted of single magnetic domains, in which all of the atomic magnetic moments are magnetized in the same direction. Single-domain particles do not have domain walls, so in the superparamagnetic (SPM) state, the entire magnetic moment of each particle is oriented in the same direction. This phenomenon is characterized by the absence of hysteresis cycles (remnant magnetization and the coercive field are null) [2]. Because of this magnetic property, SPIO nanoparticles do not interact with each other, minimizing aggregation after the field is removed. This behavior is important for *in vivo* (drug delivery, magnetic resonance imaging and magnetic hyperthermia) and *in vitro* (bioseparation, biosensing and magnetofection) biomedical applications [3–6].

The surface modification of SPIO can be carried out with alkoxysilanes via silylation reaction, in which reagents with non-hydrolyzable amino groups are commonly used. 3-Aminopropyl-triethoxysilane (APTES) is the most commonly used alkoxysilane due to its terminal amino group. The silylation process is very complex and does not involve a single mechanism. Thus, many different intermediates are possible [6–9]. Several papers have reported on the functionalization of SPIO nanoparticles with bioactive molecules through interface-containing amino groups (via APTES). The surface concentration of the bioactive molecules is correlated to the free amino group concentration, so the control of grafted APTES molecules becomes an important step in this system [7].

SPIO nanoparticles grafted with silica and alkoxysilanes to be biocompatible and to have hydrophilic properties are promising reagents in nanobiotechnology. The huge diversity of alkoxysilanes allows for different types of nanoparticle surface functionalization,

* Corresponding author. Tel.: +55 16 3301 6655; fax: +55 16 3301 6637.
E-mail addresses: r_bini11@yahoo.com.br, rafaelbini@iq.unesp.br (R.A. Bini).

0304-8853
doi:10.1016/j.jmmm.2011.08.035

i.e., introduces charges on the system that can prevent the aggregation of the particles in liquids and improve their chemical stability through surface charge control [10–12]. In addition to studying the size, structure and composition of the colloidal particles, their colloidal stability must be evaluated. Controlling the stability of the ferrofluids against aggregation is important because the formation of aggregates alters their specific surface area and dispersibility as well as their efficiency as a drug vehicle [13]. Aggregation of the nanoparticles can cause venous emboli.

In the present work, the influence of the number of alkoxide groups (hydrolyzable) in the alkoxysilanes containing the amino groups was systematically studied and correlated with the colloidal stability. The control of the free amino group density on the SPIO surface was investigated, and electrokinetic measurements in different saline concentrations were performed. The results suggest that surface charge can be controlled by grafting SPIO nanoparticles with different alkoxysilanes.

2. Materials and methods

To synthesize the iron nanoparticles, the following reactive substances were used: the iron bromine (II) and (III) ($FeBr_2$ and $FeBr_3$) (Aldrich). These chemicals were grade reactive and were used as received. For the silylation process with the iron particles, the following alkoxysilanes were used: 3-aminopropyl-triethoxysilane (APTES), 3-aminopropyl-ethyl-diethoxysilane (APDES) and 3-aminopropyl-diethyl-ethoxysilane (APES) (Aldrich). The dispersion medium was deionized (DI) water and alcohol (Aldrich). The magnetite nanoparticles were synthesized in a two-step procedure. First, nanosized magnetite (Fe_3O_4) was synthesized by a new sonoprecipitation method [14]. Second, the surface-functionalized SPIO samples were produced via hydrolysis and condensation of the organosilane agents. The nanosized magnetite was silylated using silane coupling agents in an aqueous-alcohol solution. The native nanosized magnetite sample was added to the 3-aminopropyl-triethoxysilane (APTES) aqueous-alcohol solution and refluxed at 125 °C for 2 h. The samples were then washed several times with deionized water. The sample was dried at 60 °C in a stove vacuum. The same procedure was also carried out for the alkoxysilanes 3-aminopropyl-ethyl-diethoxysilane (APDES) and 3-aminopropyl-diethyl-ethoxysilane (APES) (Fig. 1).

The electron micrographs were taken with a Philips CM 120 transmission electron microscope (TEM). Dry samples of the magnetite complexes were dispersed in isopropyl alcohol and cast onto amorphous carbon-coated copper grids for analysis. Great care was taken to ensure that both the eucentric height and focus were set consistently for each sample to reduce the uncertainty in the digital image analysis. The X-ray diffraction (XRD) pattern was recorded in a Philips powder diffractometer PW 3040/60 with Cu Kα radiation. Infrared spectra were recorded in the $4000-400\ cm^{-1}$ range on a Fourier transform infrared spectrometer (FTIR, Nicolet Instruments Corporation). To determine the surface concentration of the amino groups on the sample, the UV spectroscopy method proposed by Moon et al. [15] and adapted to nanoparticles by Marques et al. [14] was used. Dynamic light scattering (DLS) measurements were conducted with a Malvern Zetasizer Nano ZS particle analyzer (Malvern Instruments Ltd., Malvern) at a wavelength of 633 nm with a solid-state He–Ne laser at a scattering angle of 173° at 25 °C. The intensity, volume and number average diameters were calculated with the Zetasizer Nano 4.2 software utilizing an algorithm based upon the Mie theory, which transforms time-varying intensities to particle diameters [16]. For the DLS analysis, each sample was diluted to approximately 0.1 mg mL^{-1} after the solution was filtered through a Whatman Anotop alumina membrane with a pore diameter of 220 nm. The experiments were carried out at NaCl concentrations of 1×10^{-3} and 0.15 mol L^{-1} at pH 7. Each sample was analyzed directly following filtration and measured every 3 min over a 1h period. Electrokinetic measurements were also performed with a Zetasizer ZS at 25 °C, in which the measured particle velocity is due to an applied electric field that is related to the surface charge [17]. The electrokinetic measurements were taken by dispersing the sonicated samples at a concentration of 0.1 mg mL^{-1}. The ionic strength was adjusted to 1×10^{-3} mol L^{-1} NaCl. The pH was adjusted to 3.0 using 0.1 mol L^{-1} hydrochloric acid. The electrokinetic mobility was measured by increasing the pH to 12 using 0.1 mol L^{-1} sodium hydroxide. Hydrochloric acid and sodium hydroxide were determined to be in different electrolytes, and they did not greatly affect the surface charge density of the magnetite. The field-dependence magnetization (M versus H) and the temperature-dependence magnetization under zero-field cooled (ZFC) or field-cooled (FC) conditions and an applied field of 500 Oe were measured with a Quantum Design Physical Properties Measuring System (PPMS). The experimental data were normalized by the mass of the samples used in the measurements.

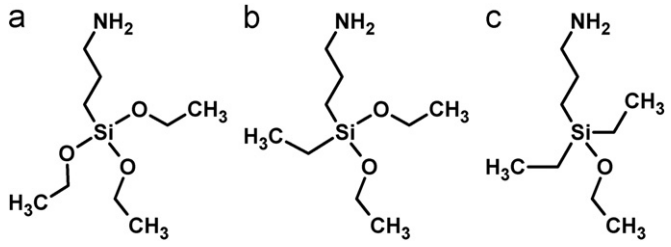

Fig. 1. Structural formulas of the alkoxysilanes used in this work. (a) APTES, (b) APDES and (APES).

3. Results and discussion

Fig. 2 shows the results of the X-ray diffraction patterns analysis of the uncoated and amino-functionalized Fe_3O_4 samples. Fig. 2(a) shows the uncoated sample. The magnetite and maghemite patterns from the JCPDS database [18] were included for comparison. Magnetite can be observed as the dominant phase; however, some maghemite may have formed during the sonoprecipitation method. The process to obtain the particles was carried out in an aqueous medium. Magnetite nanoparticles are very sensitive to oxygen. In the presence of air, some of the particles might undergo oxidation to $Fe(OH)_3$ or to the maghemite (γ-Fe_2O_3) phases [19]. The XRD pattern showed the presence of the inverse spinel structure, corresponding to either magnetite phase having a spinel structure. The presence of broad and intense peaks confirmed the formation of crystalline nanoparticles. Fig. 2(b) shows the experimental measurements of the (i) APES, (ii) APDES and (iii) APTES samples. The alkoxysilanes did not structurally change the samples. Fig. 3(a), (b) and (c) shows the TEM images of the APES, APDES and APTES samples, respectively. The electron micrographs show the nanoparticles have a nearly spherical shape with a diameter of approximately 10 nm. The average particle size was also determined from the broadening of the diffraction peaks from Scherer's equation [20]. The size was calculated to be approximately 11.6 nm, which agrees with the size estimated from the TEM images.

To confirm the grafting of the magnetite surface through the silylation reaction, an FTIR spectrum of the functionalized-magnetite was obtained (Fig. 4). The characteristic absorption bands of the Fe–O bond of the grafted SPIO shifted to higher wavenumbers, 628.7 and 577.9 cm^{-1}, compared to the uncoated SPIO

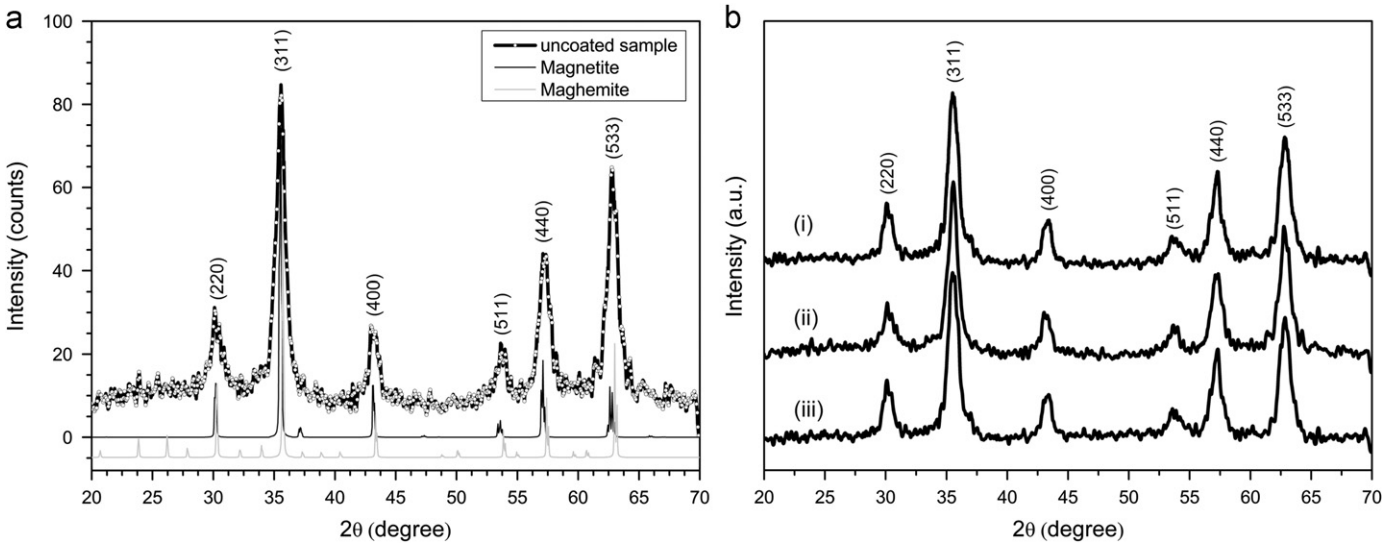

Fig. 2. X-ray powder diffraction patterns of the uncoated sample with the magnetite and maghemite patterns from the JCPDS database (a) and the APES (i), APDES (ii) and APTES (iii) samples (b).

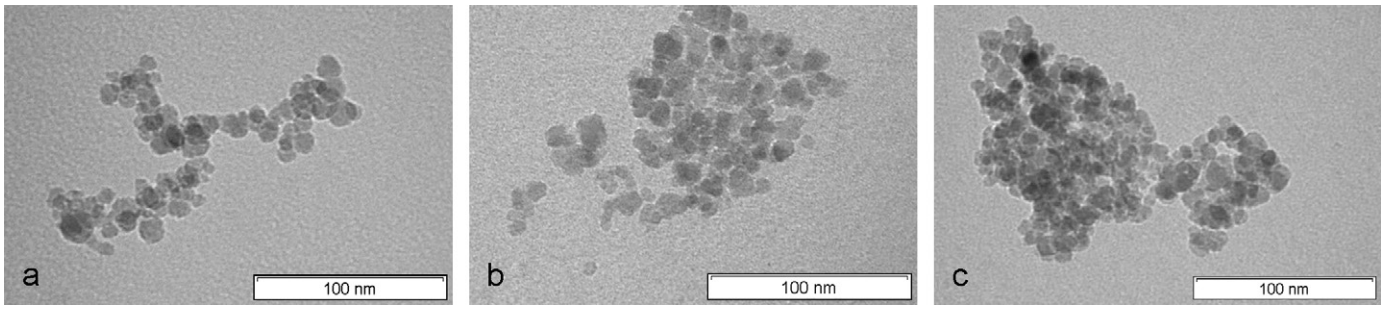

Fig. 3. TEM micrographs of the amino-functionalized Fe_3O_4 nanoparticles treated with APES (a), APDES (b) and APTES (c).

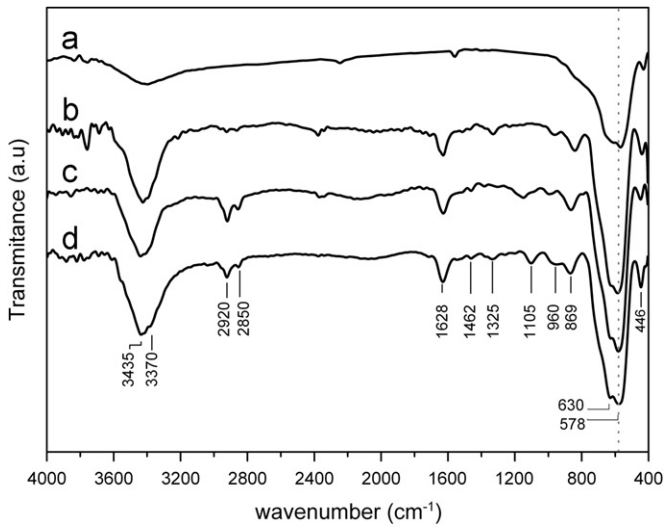

Fig. 4. The FTIR spectra of the uncoated (a), APES (b), APDES (c) and APTES (d) samples.

(in 621.4 and 574.2 cm^{-1}). This phenomenon can be explained by the formation of Fe–O–Si bonds. The Fe–O–H groups on the SPIO surface are replaced by Fe–O–Si(O–)$_2$–R as shown in Fig. 5. The greater electronegativity of –Si(O–) compared to H leads to an enhancement of the bond forces for the Fe–O bonds, shifting the absorption bands to high wavenumbers [21,22].

Surface modification by alkoxysilanes is a complex process because it does not involve a single mechanism and several experimental parameters influence the system. The FTIR spectra show the absorption bands for the silanol (Si–O–H) and siloxane (Si–O–Si) groups. Si–O stretching and Si–O–H bending vibrations at 960 and 869 cm^{-1} were observed for all of the samples. For the APTES- and APDES-coated nanoparticles, the stretching Si–O–Si was verified at 1150 – 1100 cm^{-1} [23]; however, this stretching was not observed for the APES sample, which was expected due to the presence of only one alkoxy group. The presence of amino groups associated with the 3-aminopropyl of the alkoxysilanes was observed. The absorption bands at 1325 and 2920 – 2850 cm^{-1} are ascribed to the C–N and C–H stretching vibrations, respectively. A broad band at 1628 cm^{-1} can be ascribed to the N–H stretching vibration, which is indicative of the free amino group. A small shoulder at 3370 cm^{-1} corresponds to the N–H asymmetric stretching of the amine H-bonds, indicating a possible NH_2 interaction toward the SPIO surface [23].

Table 1 shows the amino group density results. The APTES sample had the highest amino group density, and a decrease in the amino group density was observed for the APDES and APES samples. The same alkoxysilane concentration was used in each synthesis, and similar values for the amino group density on the Fe_3O_4 surface were expected, indicating the influence of the ethoxy group (–OC_2H_5) on the alkoxysilane and the presence of ethyl groups on the condensation process. Fig. 5 shows an illustration of the suggested models of alkoxysilane condensation on the SPIO surface. The polycondensation process was outstanding for the APTES molecule due to its three ethoxy groups, which

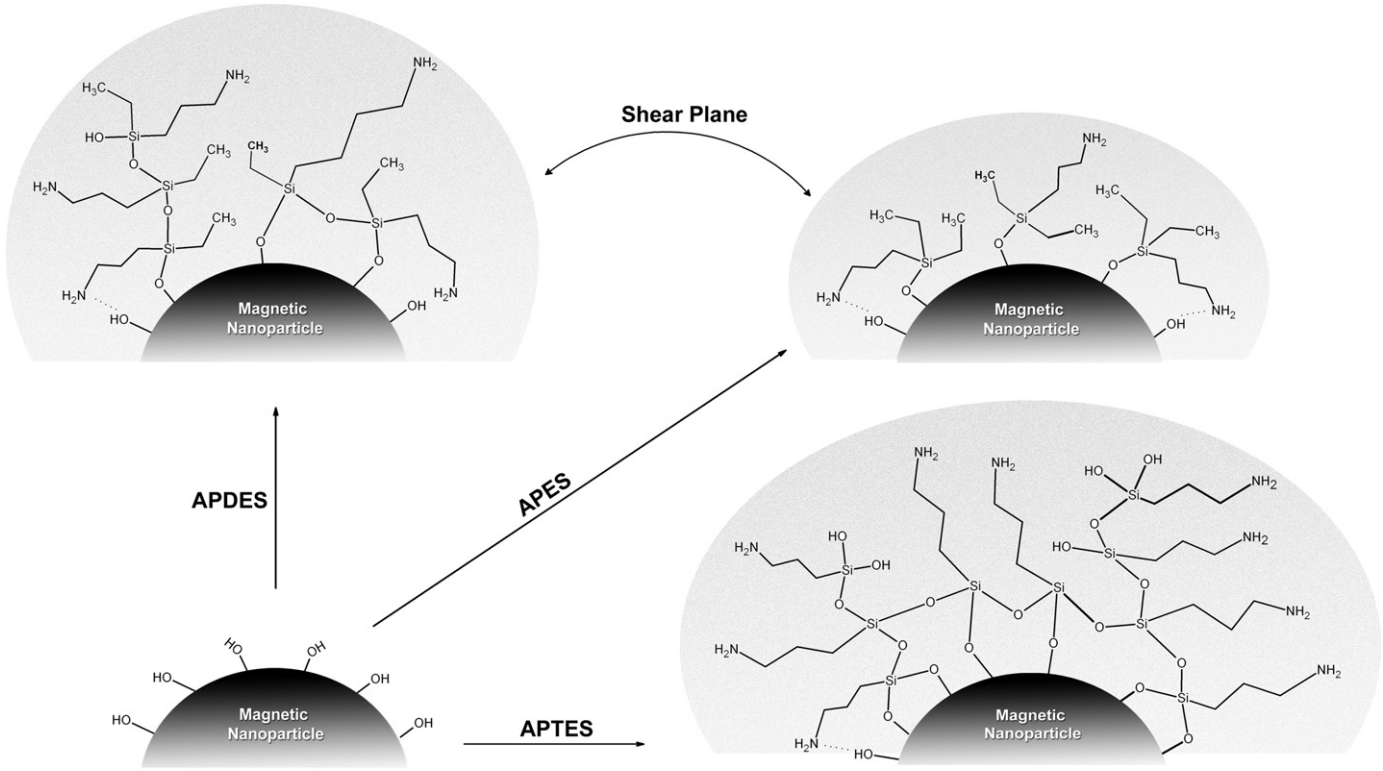

Fig. 5. Possible SPIO surfaces after coating with APTES, APDES or APES.

Table 1
Amino group density and zeta potentials of the samples.

Samples	Amino group density (nmol g^{-1})	Zeta potential (mV) at pH = 7	
		1×10^{-3} mol L^{-1} NaCl	0.15 mol L^{-1} NaCl
Uncoated	–	5.85 ± 0.21	−2.72 ± 0.25
APES	2.28 ± 0.11	12.90 ± 0.18	2.50 ± 0.21
APDES	3.20 ± 0.09	16.76 ± 0.20	3.45 ± 0.23
APTES	8.72 ± 0.07	25.05 ± 0.16	9.36 ± 0.19

contributed to the large amino group density. The APDES and APES molecules have fewer ethoxy groups. However, the ethyl groups on the APDES and APES structures cause steric hindrances, which consequently slow the condensation process and reduce the amino group density. A decrease in the amino group density may also be related to hydrogen bonding, as indicated by the FTIR spectra. The formation of H-bonded amino groups is more favored for APDES and APES than for APTES due to the smaller number of condensing groups. Thus, the free amino group can react with the surface, and intermolecular hydrogen bonds can be formed, as schematically shown in Fig. 5.

Fig. 6(a) shows the zeta potential as a function of pH for a suspension of particles in a 1×10^{-3} mol L^{-1} NaCl solution. The zeta potential curve for the synthesized nanoparticles suggests a "passive surface for the uncoated iron oxide, with the zeta potential ranging from positive values (+20 mV) at low pH values to negative values (−48 mV) at high pH values and an isoelectric point (IEP) at pH 7.30. The zeta potential of the amino-functionalized samples varied considerably with pH. At lower pH values, it was verified that the ζ-potential increased with the increase in amino group density, which correlates well with the surface concentration of the alkoxysilanes bonded to the nanoparticles, as measured by UV spectroscopy. This increase in the positive surface charge provided by the surface amino groups also results in a shift of the isoelectric point to higher pH values. APTES has an IEP at pH 10.05, which agrees with previous data [7–9]. The APDES and APES samples showed a shift to low pH with different IEP values (Fig. 6).

Fig. 6(b) and (c) shows the hydrodynamic diameters of the functionalized Fe_3O_4 samples measured by dynamic light scattering in 0.0010 and 0.15 mol L^{-1} NaCl at pH 7. Upon increasing the electrolyte concentration, the slope of the hydrodynamic diameter versus time curve increases. The uncoated sample showed lower stability than the coated samples for both NaCl concentrations. By comparing Fig. 6(b) and (c), the increased electrolyte concentration induced the formation of larger aggregates by suppressing the double-layer repulsion between the particles. According to the Derjaguin and Landau, Verwey and Overbeek (DLVO) theory, the electrical double-layer thickness ($1/\kappa$) repulsion decreases with increasing salt concentrations [24,25]. In this work, the hydrodynamic diameters (i.e., the inverse of the Debye–Hückel parameter ($1/\kappa$) [24]) of the samples measured in 0.0010 and 0.15 mol L^{-1} NaCl at 298 K were 13.6 and 1.1 nm, respectively. These $1/\kappa$ values agree with the zeta potential values in Table 1, and they help to explain the different behaviors in Fig. 6(b) and (c).

Fig. 6(b) shows that the APTES coating resulted in fewer aggregates because of the large charge density on the surface, as shown in Table 1. However, APES ($\zeta = +12.90$ mV) had smaller aggregates than the APDES sample ($\zeta = +16.76$ mV). This finding was not expected due to the difference in the surface potentials. This behavior was also observed in the samples measured in 0.15 mol L^{-1} NaCl. Fig. 6(c) shows that the nanoparticles treated with APES ($\zeta = +2.50$ mV) had smaller aggregates than the other amino-functionalized samples with greater zeta potentials, such as APTES ($\zeta = +9.36$ mV). These samples have low surface potentials, and the aggregation could be a spontaneous process in the system. In addition to hydrodynamic diameter measurements,

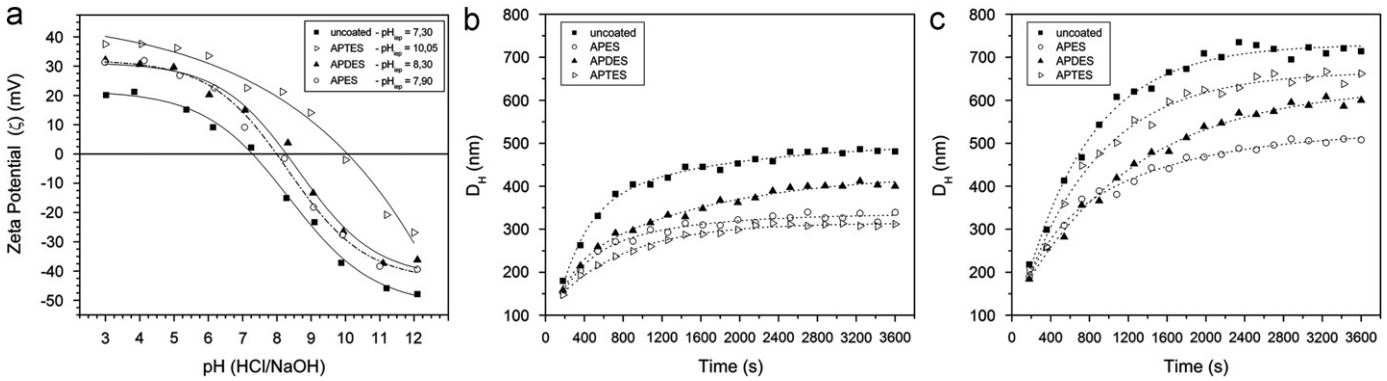

Fig. 6. (a) The zeta potential of the amino-functionalized Fe_3O_4 particles in the 1×10^{-3} mol L^{-1} NaCl solution. The hydrodynamic diameters of the samples measured by dynamic light scattering plotted versus time for 1×10^{-3} and 0.15 mol L^{-1} NaCl at pH 7, respectively (b) and (c).

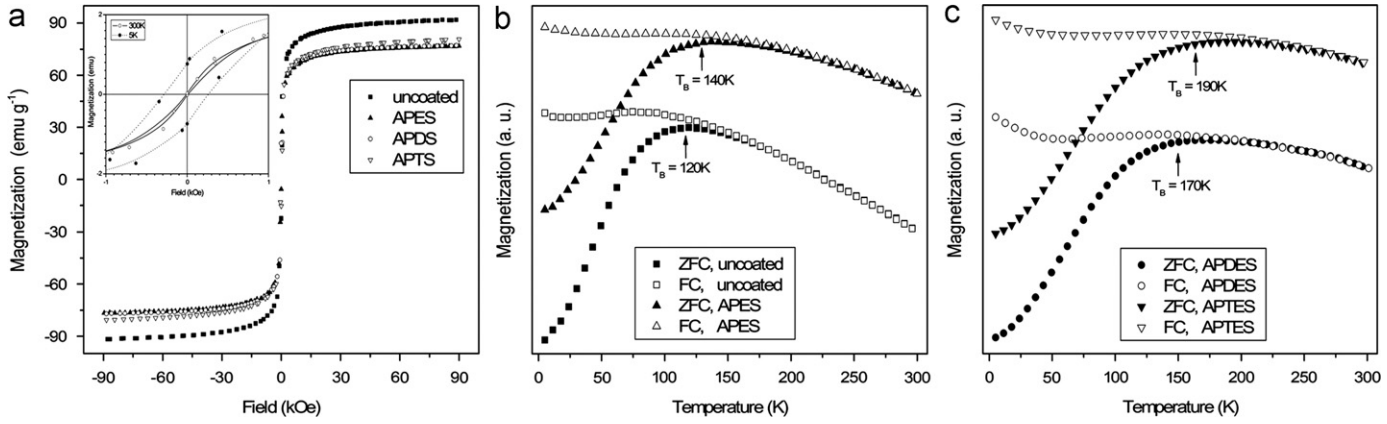

Fig. 7. (a) *M* versus *H* plot of the uncoated and amino-functionalized Fe_3O_4 samples at 300 K. Inset *M* versus *H* plot of the uncoated sample at the low-field region showing coercivity. The unit emu g^{-1} represents the magnetization, which was normalized by the mass of the samples in the measurements. The ZFC–FC plots showing the blocking temperature (b) and (c).

DLS can be used to determine the polydispersity index (PDI) of a dispersion. Higher PDI values were obtained for the uncoated sample: 0.3054 and 0.4286 in 0.0010 and 0.15 mol L^{-1} NaCl at pH 7, respectively. For the amino-functionalized samples, the polydispersity values agree with the hydrodynamic diameters, slopes and the zeta potentials. For the APTES sample, the observed PDI values were 0.1765 and 0.3934 for 0.0010 and 0.15 mol L^{-1} NaCl, respectively. For the APDES samples, the PDI values were 0.2629 and 0.3538 for 0.0010 and 0.15 mol L^{-1} NaCl, respectively. For the APES samples, the PDI values were 0.1835 and 0.3249 for 0.0010 and 0.15 mol L^{-1} NaCl, respectively. The influence of the ethyl groups of the APDES and APES molecules is evident. The ethyl groups provide steric stabilization, generating an electrosteric system that confers proportionally larger stability as compared to the electrostatic stabilization by APTES.

Fig. 7 shows the magnetic measurements of the uncoated and functionalized Fe_3O_4 samples. At 300 K, SPM behavior was registered. The samples did not exhibit hysteresis, and neither coercivity nor remanence was detected (Fig. 7(a)). Ferromagnetic behavior with a coercivity of about 280 Oe is observed at 5 K for the uncoated sample (inset of Fig. 7a). This behavior was also observed for the functionalized Fe_3O_4 samples. The saturation magnetizations of samples were found to be 80.45, 65.05, 65.45 and 68.82 emu g^{-1} for the uncoated, APES, APDES and APTES samples, respectively.

The temperature dependence of the magnetization *M*(T) was taken in ZFC and FC conditions (Fig. 7b and c). The maximum in the ZFC curve defines the blocking temperatures, at which the thermal energy becomes comparable to the anisotropy energy barrier [26]. The blocking temperatures (T_B) for the uncoated, APES, APDES and APTES samples were verified to be approximately 120, 140, 170 and 190 K, respectively. The blocking temperatures changed due to the different alkoxysilanes on the surface. The blocking temperatures of the SPIO nanoparticles depend on the surface state, interparticle interactions, size and size distribution [26]. The contributions to the anisotropy energy can originate from the intrinsic anisotropies of the particles (shape, magnetocrystallinity or stress anisotropies) or interparticle interactions (dipolar or exchange). Separating these effects is difficult [27]. The same procedure was carried out for all of the samples. Thus, any increases in T_B could be ascribed to the addition of the alkoxysilanes into the system. The FTIR, zeta potential and amino group density analyses indicate that ($-OC_2H_5$) condensation was more effective for APTES. The increase in this condensation can increase the interparticle aggregation, leading to the formation of larger aggregates particles. The ZFC/FC measurements are sensitive to changes in the size distribution of the system (Fig. 7(b) and (c)). The formation of larger aggregates also can be verified by the *y*-shaped curves. Below the T_B, the magnetization decreases for the ZFC, while for FC, the magnetization increases. This behavior is normally ascribed to interparticle interactions with some degree of agglomeration [28].

4. Conclusions

Superparamagnetic iron oxide particles coated with alkoxysilanes were successfully synthesized. A decrease in the number of alkoxides ($-OC_2H_5$) on the surface caused a decrease in the concentration of free amino groups on the SPIO surface. The electrokinetic

measurements, which showed that the IEP shifted for smaller values of pH, provided evidence concerning the effect of the surface amino group. The DLS measurements in 0.15 mol L^{-1} NaCl showed that APDES and APES, with smaller amino group densities and zeta potentials, impart greater stability than APTES, which has a larger surface potential. The main difference among the samples was the alkoxy group number, relative to APTES. APDES has the insertion of an ethyl group, while APES has two ethyl groups. Therefore, the decrease in the concentration of the free amino group and zeta potential shifts can be related to the reactivity of the molecules. The shifts in the blocking temperatures show that the concentration of alkoxides ($-OC_2H_5$) on the functionalized molecules affects interparticle aggregation. The differences in the colloidal stability are due to steric contributions provided by the ethyl groups. This work examined the influence of alkoxyl groups on the colloidal stability of surface-modified SPIO nanoparticles. Future studies will have to be conducted. The magnetic properties and colloidal stability of the nanoparticles in a physiological saline solution were correlated with the interparticle interactions due to the different shell configurations on the SPIO surface. Colloidal stability is an extremely important parameter for *in vivo* SPIO biomedical applications and helps to inhibit capillary emboli when carrying biological molecules or drugs.

Acknowledgements

This work was supported by the CNPq and FAPESP Brazilian Agencies.

References

[1] I.W. Hamley, Angewandte Chemie International Edition 42 (2003) 1692.
[2] G.F. Goya, V. Grazú, M.R. Ibarra, Current Nanoscience 4 (2008) 1.
[3] M. Mikhaylova, D.K. Kim, C.C. Berry, A. Zagorodni, et al., Chemistry of Materials 16 (2004) 2344.
[4] A.K. Gupta, M. Gupta, Biomaterials 26 (2005) 3995.
[5] D. Zhang, Z. Tong, S.Z. Li, X.B. Zhang, A. Ying, Materials Letters 62 (24) (2008) 4053.
[6] C. Zhang, B. Wangler, B. Morgenstern, H. Zentgraf, Langmuir 2 (2007) 1427.
[7] S. Campelj, D. Makovec, M.J. Drofenik, Journal of Magnetism and Magnetic Materials 321 (2009) 1346.
[8] Z. Xu, Q. Liu, J.A. Finch, Applied Surface Science 120 (1997) 269.
[9] I.J. Bruce, T. Sen, Langmuir 21 (2005) 7029.
[10] L.N. Donselaar, A.P. Philipse, J. Suurmond, Langmuir 13 (1997) 6018.
[11] Q. Liu, Z. Xu, J.A. Finch, R. Egerton, Chemistry of Materials 10 (1998) 3936.
[12] M.A. Correa-Duarte, M. Giersig, N.A. Kotov, L.M. Liz-Marzan, Langmuir 14 (1998) 6430.
[13] S.A. Gomez-Lopera, J.L. Arias, V. Gallardo, A.V. Delgado, Langmuir 22 (2006) 2816.
[14] R.F.C. Marques, T.P. Costa, L.C. Varanda, N.J.J.Silva, F.J. Santos, A. Milan, M. JafelicciJr., in: Proceedings of the Sixth Encontro SBPMat 2007, Natal. Abstracts, SBPMat, São Paulo, 2007 p. D579.
[15] J.H. Moon, J.H. Kim, K. Kim, T. Kang, et al., Langmuir 13 (1997) 4305.
[16] Zetasizer Nano Series User Manual, Malvern Instruments: Worcestershire, UK, 2005.
[17] DTS Support Disk: Colloids and Zeta Potential, Malvern Instruments: Worcestershire, UK, 2005.
[18] Joint Committee for Powder Diffraction Studies—Diffraction Data Base. Newton Square: International for Diffraction Data, 2005.
[19] R.M. Cornell, U. Schwertmann, The iron oxides: structure, properties, reactions, occurences and uses, 2nd ed., VHC, Weinheim, 2003 694 p.
[20] J.I. Langford, A.J.C. Wilson, Journal of Applied Crystallography 11 (1978) 102.
[21] M. Ma, Y. Zhang, W. Yu, et al., Colloids and Surfaces A—Physicochemical and Engineering Aspects 212 (2003) 219.
[22] W.S. Wei, J. Yang, T.J. Wang, et al., Acta Physico Chimica Sinica 17 (2001) 507.
[23] L.D. White, C.P. Tripp, Journal of Colloid and Interface Science 232 (2000) 400.
[24] R.J. Hunter, Foundations of Colloid Science, 3rd ed., Clarendon Press, Oxford, 1989.
[25] M. Di Marco, I. Guilbert, M. Port, et al., International Journal of Pharmaceutics 331 (2007) 197.
[26] B.D. Cullity, Introduction to Magnetic Materials, 2nd ed., Addison- Wesley, MA, 1972, pp. 94, 389–414.
[27] L.F. Gamarra, W.M. Pontuschka, J.B. Mamani, et al., Journal of Physics—Condensed Matter 21 (2209) 115104.
[28] V. Kusigerski, M. Tadic, V. Spasojevic, et al., Scripta Materialia 56 (2007) 883.